ARMY RESEARCH LABORATORY

A One-Dimensional Atmospheric Boundary Layer Model: Intermittent Wind Shears and Thermal Stability at Night

Arnold Tunick

ARL-MR-494

June 2001

The findings in this report are not to be construed as an official Department of the Army position unless so designated by other authorized documents.

Citation of manufacturer's or trade names does not constitute an official endorsement or approval of the use thereof.

Destroy this report when it is no longer needed. Do not return it to the originator.

Army Research Laboratory

Adelphi, MD 20783-1197

ARL-MR-494 **June 2001**

A One-Dimensional Atmospheric Boundary Layer Model: Intermittent Wind Shears and Thermal Stability at Night

Arnold Tunick

Computational and Information Sciences Directorate

Abstract

A one-dimensional, time-dependent computer model of the atmospheric boundary layer was developed to simulate intermittent turbulence and the near-ground microclimate under nighttime stable conditions. In this study, the model produced several turbulent events (oscillations) through the nighttime period that varied in number, frequency, and strength along the axes of initial geostrophic wind speed. These results were found to be in close agreement with results from several previous observational and theoretical studies of this type. It is suggested, therefore, that the one-dimensional computer model is a useful mathematical representation of the nighttime case that includes intermittency.

Contents

Figures

Tables

1. Introduction

Field experimenters have frequently observed turbulent "bursts" in the lower boundary layer, suggesting that they are likely the result of gravity-wave activity and other wind-shear or thermal instabilities (e.g., Schubert, 1977; Lu et al, 1983; Coulter, 1990; Nappo, 1991; Weber and Kurzeja, 1991; and Blumen et al, 1999). Such turbulent events have even been linked to particular mesoscale events and synoptic situations, like outflow from nearby thunderstorms, as reported in Zhou Ming-yu et al (1980) and Neff (1980). In contrast, atmospheric computer modelers (e.g., Blackadar, 1979; McNider and Pielke, 1981; Lin, 1990; ReVelle, 1993; and McNider et al, 1995) describe time-dependent oscillations at night as resulting from nonlinear interactions between the ground surface and the airflow aloft. From the modeler's point of view, several external parameters, in the right combination, can increase the chances for a model to produce intermittent turbulence during the nighttime period. These parameters are typically surface roughness, initial soil moisture or heat capacity, and geostrophic (upper level) wind speed. Since intermittent "bursts" of turbulence in the lower boundary layer cause wind gusts and fluctuations in temperature, much attention has been directed toward nighttime cases that include intermittency in modeling atmospheric pollution (Nappo and Bach, 1997; Nappo and Johansson, 1998).

Model results for the nighttime case that includes intermittency have been shown in previous works, e.g., Lin (1990) and ReVelle (1993), along with descriptions of the parameter space within which time-dependent oscillations occur. From these earlier discussions, however, it is not clear to what extent variations initial geostrophic wind speed, surface roughness, and soil moisture affect the onset and cycling of wind shear and thermal instabilities at the surface and aloft. In this report, therefore, the author presents an expanded and improved view of the nighttime intermittently stable solution within the continuum of several varying model parameters. The author provides incremental time series of potential temperature and wind speed as well as time-height series of the derived momentum and heat flux for the layers $2 \leq z \leq 150$ m .

2. The Atmospheric Boundary-Layer Model

The one-dimensional, time-dependent model used in this study is based on the previous works of Pielke and Mahrer (1975), McNider and Pielke (1981), and Avissar and Mahrer (1988). It is a first-order, local-turbulence closure computer model formulated to calculate the transfer of momentum, heat, and moisture at the surface and aloft. The model uses an implicit finite difference scheme to integrate the boundary layer and soil-diffusion equations and contains many detailed formulations for the surface-energy budget. The model's surface-layer turbulence scaling is as described by Zilitinkevich (1970) and Businger et al (1971). A formulation suggested by Smeda (1979) is used for the time-dependent calculation of the depth of the nighttime stable layer. Table 1 summarizes the model parameters for this study of the lower nighttime boundary layer.

Table 1. Nighttime boundary-layer model parameters.

Number of vertical levels	19 (2, 5, 15, 30, 80, 150, 208, 445, 690, 943, 1203, 1470, 1743, 2023, 2311, 2609, 2916, 3250, 3500 m)
Latitude, longitude	45.0 N, 0.0 E
Surface roughness	0.28 m
Canopy height	2.0 m
Surface emissivity	0.95
Soil water content	0.1 m^3/m^3
Average soil density	1400 kg/m^3
Soil texture (% sand, % clay, % organic)	28.0, 70.0, 2.0
Geostrophic wind speed	u_g = 6.5, 8.0, 9.5 m/s ; v_g = 0.0 m/s
Day of the year	91
Initial time (sunset)	~18 local time
Initial potential temperature in the surface layer	~284.0 K
Time step	3 s

The model equations for the time-dependent calculation of the winds (u- and v-components), potential temperature (θ), and specific humidity (q) over flat earth can be expressed as

$$\frac{\partial \bar{u}}{\partial t} = f\left(\bar{v} - v_g\right) + \frac{\partial}{\partial z}\left(K_m \frac{\partial \bar{u}}{\partial z}\right) \tag{1}$$

$$\frac{\partial \bar{v}}{\partial t} = f\left(u_g - \bar{u}\right) + \frac{\partial}{\partial z}\left(K_m \frac{\partial \bar{v}}{\partial z}\right) \tag{2}$$

$$\frac{\partial \bar{\theta}}{\partial t} = \frac{\partial}{\partial z}\left(K_h \frac{\partial \bar{\theta}}{\partial z}\right), \text{ and} \tag{3}$$

$$\frac{\partial \bar{q}}{\partial t} = \frac{\partial}{\partial z}\left(K_q \frac{\partial \bar{q}}{\partial z}\right) \tag{4}$$

where f denotes the Coriolis parameter, subscript g refers to the geostrophic wind, K_m denotes the turbulence transfer coefficient for momentum, and $K_h = K_q$ denotes the transfer coefficients for heat and moisture. In the surface layer, K_m and K_h are calculated as $K_m = ku_*z/\phi_m$ and $K_h = ku_*z/\phi_h$, respectively, where k is Kármán's constant, z is height above ground level (agl) (in meters), u_* is the friction velocity (in units of m/s), and ϕ_m and ϕ_h are nondimensional lapse-rate functions that account for surface-layer stabilities other than neutral. A list of symbols is provided in the appendix.

During the nighttime, when the surface layer is generally stable, that is, $\theta_* > 0$, where $\theta_* = \frac{kz}{\phi_h}\frac{\partial \theta}{\partial z}$ is the potential temperature scaling constant, the model derives the diffusion coefficients above the surface layer as suggested by Blackadar (1979)

$$K_m(z) = K_h(z) = \begin{cases} sl^2(1-18Ri)^{0.5}, & Ri < 0 \\ sl^2\left(Ri_{crit} - Ri\right)/Ri_{crit}, & 0 < Ri \le Ri_{crit} \\ 0, & Ri > Ri_{crit} \end{cases}, \tag{5}$$

where s is the local wind shear, The parameter, Ri, called the Richardson number, is the ratio of thermal to mechanical (wind shear) production of turbulent energy, so that $Ri = \frac{g}{\theta}\frac{\partial \theta}{\partial z}\Big/\left(\left(\partial u/\partial z\right)^2 + \left(\partial v/\partial z\right)^2\right)$. Ri_{crit} is the limiting value of the Richardson number, where it is often assumed that $Ri_{crit} = 0.25$. Alternatively, $Ri_{crit} = 0.115\Delta z^{0.175}$ (McNider and Pielke, 1981; Avissar and Mahrer, 1988), where Δz is the model grid spacing in centimeters. This expression results in having values approaching 0.25 for finer

grid spacing and values closer to 0.65 where the grid is more coarse (i.e., 150 to 250 m). The length, l (in meters), $l = kz\left(1+\frac{kz}{0.0063u_*/f}\right)^{-1}$ is generally thought of as the width of turbulence and is characterized by this formulation reported in Blackadar (1979), for z above the surface layer. As mentioned earlier, the formulation suggested by Smeda (1979) for the depth of the nighttime planetary boundary layer, z_i, is calculated as

$$\frac{dz_i}{dt} = 0.06\frac{u_*^2}{z_i f}\left[1 - \left(\frac{3.3z_i f}{u_*}\right)^3\right]. \tag{6}$$

Some previous results obtained with the use of this expression for the depth of the nighttime planetary boundary layer were in good agreement in comparison to the observed data (Tunick, 2000).

The surface-energy budget as described by Pielke (1984) and Avissar and Mahrer (1988) can be written as

$$(1-A)R_{s\downarrow} + R_{L\downarrow} - R_{L\uparrow} - \rho c_p u_* \theta_* - \rho L_v u_* q_* + Q_s = F \ , \tag{7}$$

where A is surface reflectivity (albedo); $R_s\downarrow$, $R_L\downarrow$, and $R_L\uparrow$ are the incoming solar, incoming long-wave, and outgoing long-wave radiative fluxes, respectively; u_*, θ_*, and q_* are the surface-layer turbulence scaling parameters for wind speed, temperature, and moisture, in that order; ρ is the air density; c_p is the specific heat of air at constant pressure; L_v is the heat of transformation for water vapor; Q_s is the soil heat flux; and F is the function applied in solving iteratively for the surface temperature. The formulation for downward long-wave radiation is based on the earlier works reported by Paltridge and Platt (1976), which can be expressed as

$$R_{L\downarrow} = -170.9 + 1.195\,\sigma\,T_r^4 + 0.3\,cld\,\varepsilon_c\,\sigma\,T_c^4 \ , \tag{8}$$

where $\sigma = 5.6697 \times 10\text{-}8$ W m^{-2} deg^{-4}, T_r is the reference level (~2 m) temperature in kelvins, cld is the cloud amount, ε_c, is the emissivity of the cloud base, and T_c is the temperature of the cloud base in kelvins. This expression has worked quite well in two previous studies (i.e., Rachele and Tunick, 1994; Tunick et al, 1994).

Integration of the partial differential equations (1) to (4) is achieved with a generalized form of the Crank-Nicholson implicit finite difference scheme (Paegle et al, 1976; also see Pielke, 1984, sect. 10.1.2, and Ahlberg et al, 1967). Boundary conditions applied at the top of the model are such that the variables retain their initial values.

3. Model Results

As reported in Businger (1973), McNider et al (1995), and Mahrt (1998), the following events frequently characterize the nighttime stable boundary layer:

(a) Strong surface radiative cooling and the formation of a stably stratified layer near the ground.

(b) Suppressed turbulence as the ground cools and the development of a laminar layer.

(c) Heat and momentum transfer of from higher layers is blocked and the Richardson number exceeds its critical value at some height above the ground.

(d) Surface wind speeds decrease (calm). The nocturnal low-level jet intensifies.

(e) Above the laminar layer, momentum continues to be transferred downward.

(f) Above the laminar layer, little heat is exchanged since the thermal gradient at this level is close to neutral.

(g) If there is very strong thermal stability at the surface, the airflow aloft may, in effect, become disconnected or decoupled from it.

(h) Winds above the laminar layer will continue to accelerate in the absence of surface friction.

(i) Temperatures at the surface will continue to decrease.

(j) Wind shears above the laminar layer will build up in the absence of offsetting heat flux.

(k) The Richardson number begins to decrease below its critical value. The laminar surface layer will be eroded from above by wind shears.

(l) Downbursts of turbulence cause wind gusts and oscillations in temperature (and moisture). Vertical mixing depletes strong wind shears.

(m) The series of events (a) through (l) repeats itself through the nighttime period. This is the intermittently stable nighttime case.

(n) If, however, winds and wind shears are initially strong through the lower nighttime boundary layer, a more turbulently mixed, weakly stratified layer is maintained.

(o) Windier and warmer conditions at the surface will prevail. This is the coupled nighttime boundary-layer solution.

Figure 1 shows the coupled, decoupled, and intermittently stable nighttime results for (a) potential temperature and (b) modeled wind speed in the surface layer at 5 m agl. The dashed, circled, and solid lines are for levels of stability corresponding to three different initial values of geostrophic wind speed, i.e., 6.5, 8.0, and 9.5 m/s, respectively. Where turbulence is maintained by strong wind shears (dashed line), temperatures and wind speeds in the surface layer remain high and highly coupled to the air aloft. Where turbulence is suppressed by strong thermal stability (solid line), the model produces lower surface temperatures* and lower wind speeds. The intermittently stable solution (circled line) clearly oscillates between the coupled (windier, warmer) and decoupled (calmer, cooler) states. Figure 1 of the

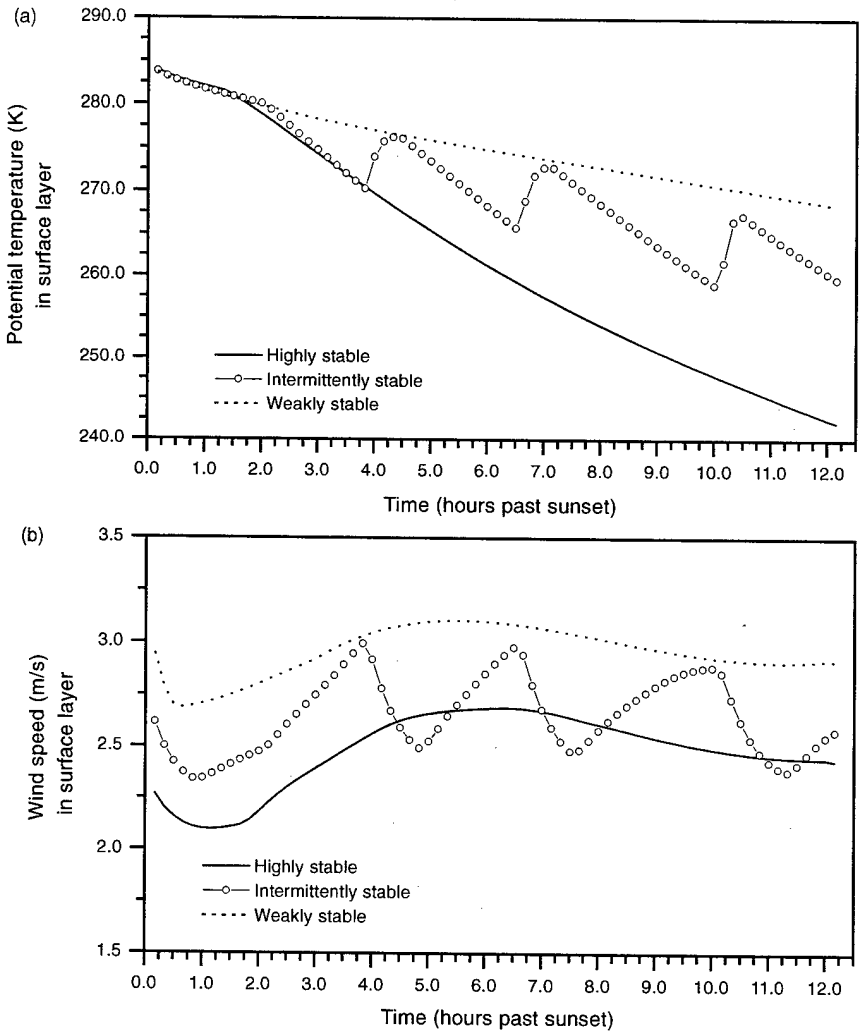

Figure 1. Line plot of potential temperature (K) at 5 m agl in surface layer (a) and wind speed (m/s) at 5 m agl in surface layer (b) for values of geostrophic wind speed of 6.5 (solid line), 8.0 (circled line), and 9.5 m/s (dashed line).

* Certainly, the temperature results in figure 1 are unrealistically low. The so-called "runaway" cooling (as expressed by Mahrt, 1998) is apparently a common defect in numerical models that calculate meteorological gradients near the ground at night with the use of Obukhov similarity functions (Monin and Obukhov, 1954). In this situation, not enough heat is transferred from aloft to offset steady radiative and surface losses.

present study looks very similar to ReVelle's (1993) figures 3 and 4, where, over a period of 16 hours, four oscillations in temperature and wind speed were shown to occur at approximately 4.0, 7.5, 10.5, and 13.0 h past sunset. In this example, three oscillations occurred (over a period of 12 hours) at approximately 3.75, 6.5, and 10.0 h past sunset, which is in close agreement with ReVelle's results. By this example, the model is also found to be in close agreement with several other observational and theoretical results (reported in the literature) on nighttime downburst events. Table 2 gives a comparative summary of the current and previous results.

Figure 2 contains data from several consecutive model runs (i.e., fig. 2 contains fig. 1). The incremental time series of potential temperature (a) and wind speed (b) in the surface layer at 5 m agl show that several oscillations are generated through the nighttime period that vary greatly in number, frequency, and strength along the axes of initial geostrophic wind speed. Figure 2 shows that the onset of such events, in hours past sunset, also varies along this dimension. The numbers of oscillations that occur are shown to increase from 1 to 8 or more in the direction of increasing of geostrophic winds. At the same time, as the total numbers of oscillations increase, their intensity or strength tends to decrease. Figure 2 also indicates where the decoupled nighttime solution occurs (i.e., an extreme depression in temperature and calmer winds, as explained above). In contrast, the coupled nighttime boundary-layer solution is indicated where temperatures decrease less severely. An unexpected result for this case is that the model produces oscillations in two cycles. This result is interesting because it suggests that a layer with sufficiently strong wind speeds and wind shears can become intermitently turbulent at even higher windspeeds under the right set of conditions.

Table 2. Summary of previous observational and theoretical results on nighttime "bursting" events.

Source [a]	Type (O/T)[b]	Surface roughness (m)	Geostrophic wind speed (m/s)	Average number of events per night
Thorpe and Guymer (1977)	O	not indicated	< 10.0	3 h^{-1} per event
Schubert (1977)	O	~1.5	not indicated	1–2 within ~5 h
Blackadar (1979)	T	1.0	8.0	5–6
Coulter (1990)	O	0.1–1.0	not indicated	4–5
Lin (1991)	T	1.0	8.0	2–3
Nappo (1991)	O	0.1–1.0	not indicated	13–18
Revelle (1993)	T	0.1–1.0	1.0–3.0	3–8
Present study [c]	T	0.28 (0.1–1.0)	8.0 (3.0–11.0)	3 (1–8)

[a]Adapted from ReVelle (1993), table 2, p. 1177.

[b]O–observations; T–theory.

[c]Numbers inside the parentheses are implied from the model results shown in figures 2, 5, and 6.

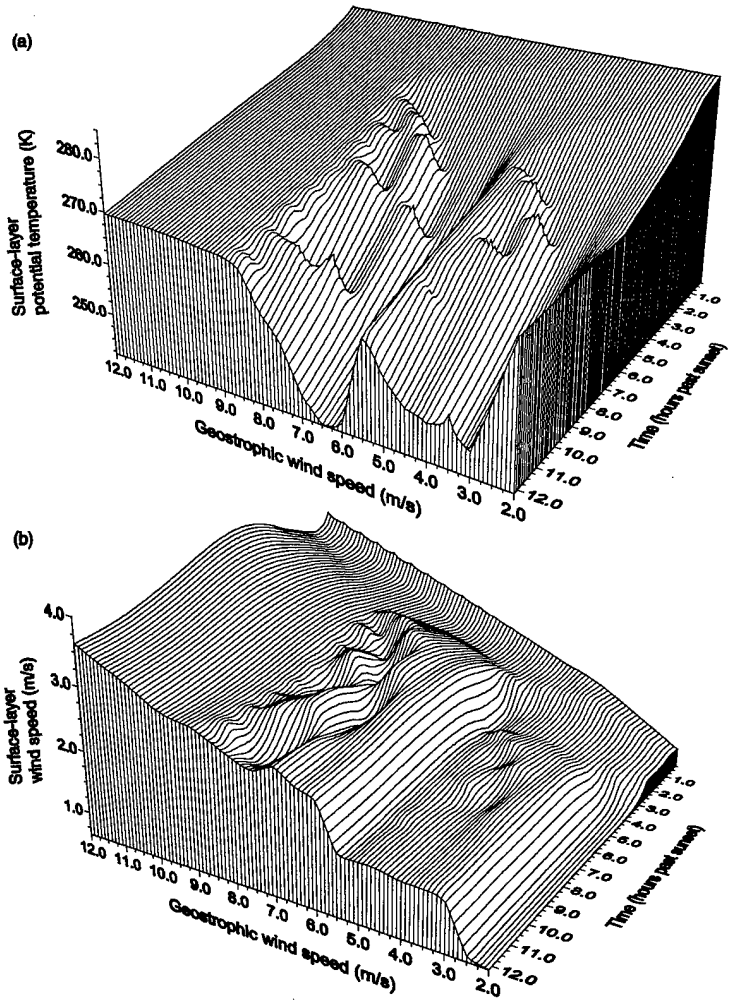

Figure 2. Surface plot of potential temperature (K) at 5 m agl in surface layer (a) and wind speed (m/s) at 5 m agl in surface layer (b) as a function of time past sunset and value of initial geostrophic wind speed.

Figures 3 and 4 show times series of potential temperature data and wind speed data, respectively, at 15, 30, 80, and 150 m agl. Away from the surface ($z > 30$ m), temperatures and wind speeds are shown to change very little through the nighttime period when geostrophic wind speeds are low and heat transfer is limited. In contrast, when initial geostrophic wind speeds are higher and turbulent transfers of heat and momentum are maintained, potential temperatures are shown to decrease steadily through the nighttime period. Figures 3 and 4 also show that oscillations are affected through the entire layer ($z \leq 150$ m), although additional evidence regarding the onset of the instabilities would be desirable.

Figure 5 is similar to figure 2 except that it shows the model results as they are affected by changes in surface roughness, that is, $z_0 = 0.01$ m (fig. 5(a) and 5(c)) and $z_0 = 1.0$ m (fig. 5(b) and 5(d)). (In calculating the data in figure 2, $z_0 = 0.28$ m.) These results show that the surface layer tends toward warmer temperatures (approximately 8 to 10 K) and calmer wind speeds (approximately 2 to 3 m/s) as surface roughness increases from 0.01 to 1.0 m. This is likely due to increased surface stress (Munn, 1966). The results also show

Figure 3. Surface plot of potential temperature (K) at (a) 15, (b) 30, (c) 80, and (d) 150 m agl in lower boundary layer as a function of time past sunset and value of initial geostrophic wind speed.

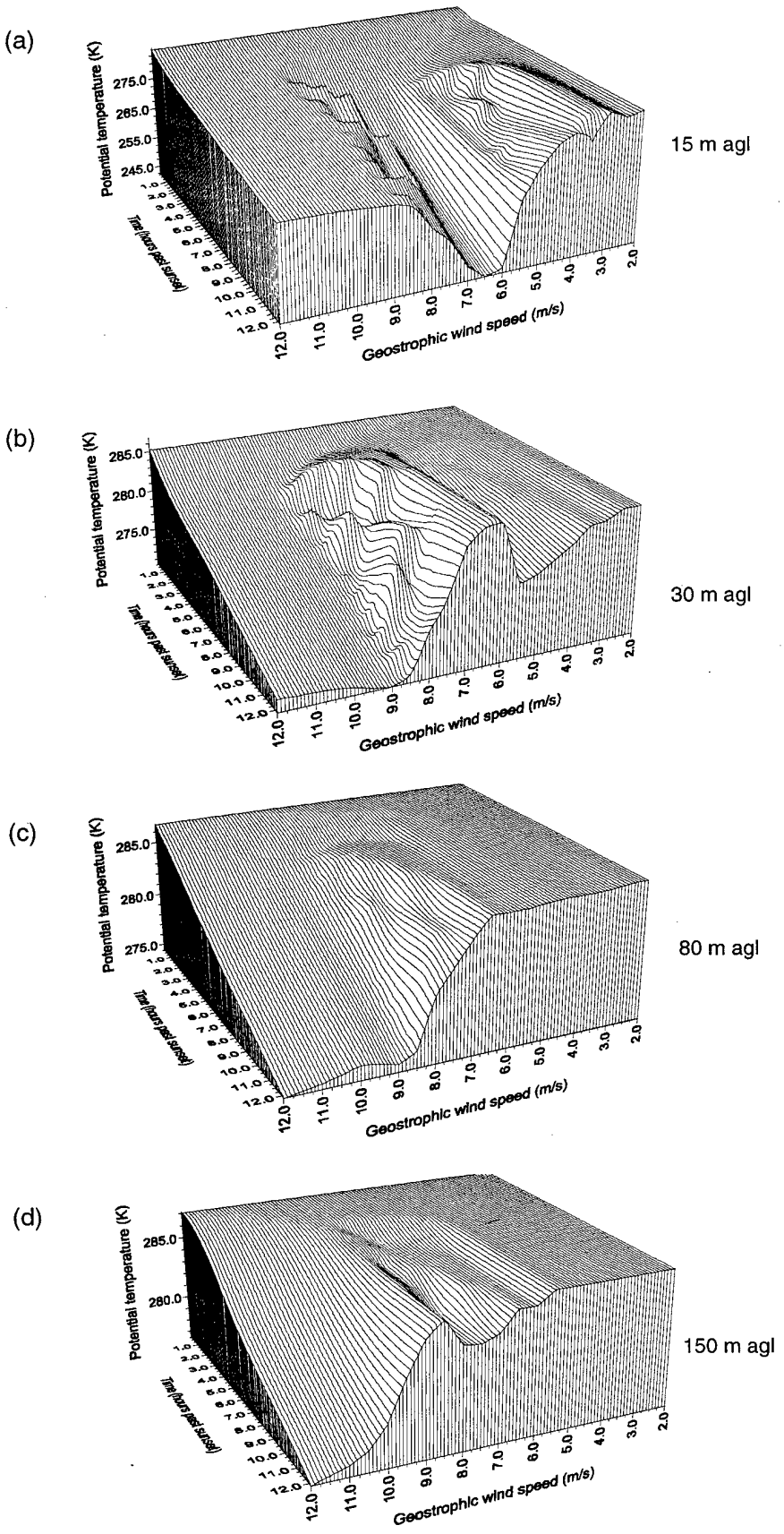

Figure 4. Surface plot of wind speed (m/s) at (a) 15, (b) 30, (c) 80, and (d) 150 m agl in lower boundary layer as a function of time past sunset and value of initial geostrophic wind speed.

(a)

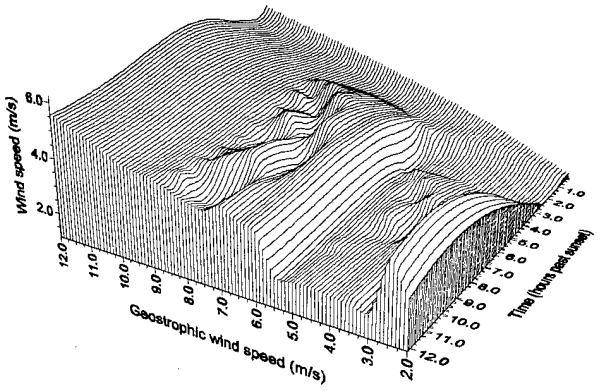

15 m agl

(b)

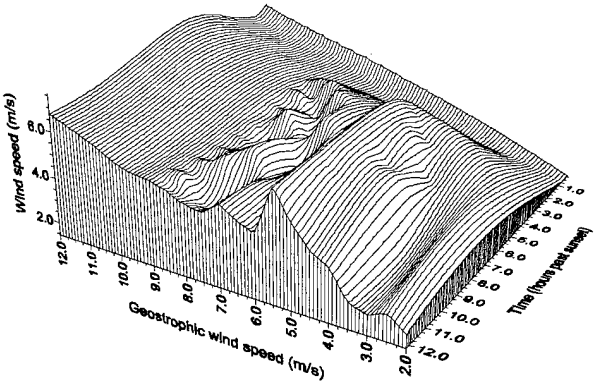

30 m agl

(c)

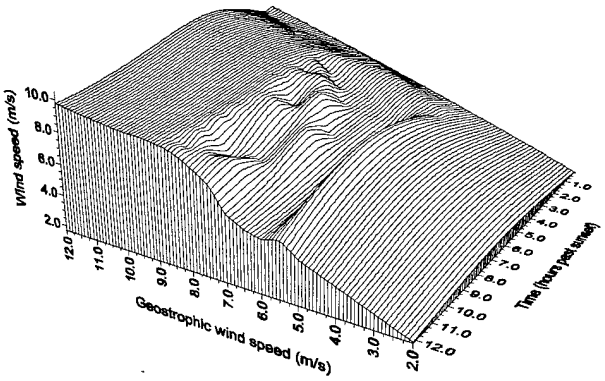

80 m agl

(d)

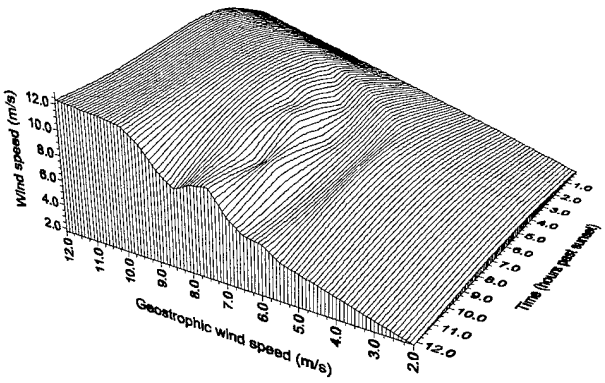

150 m agl

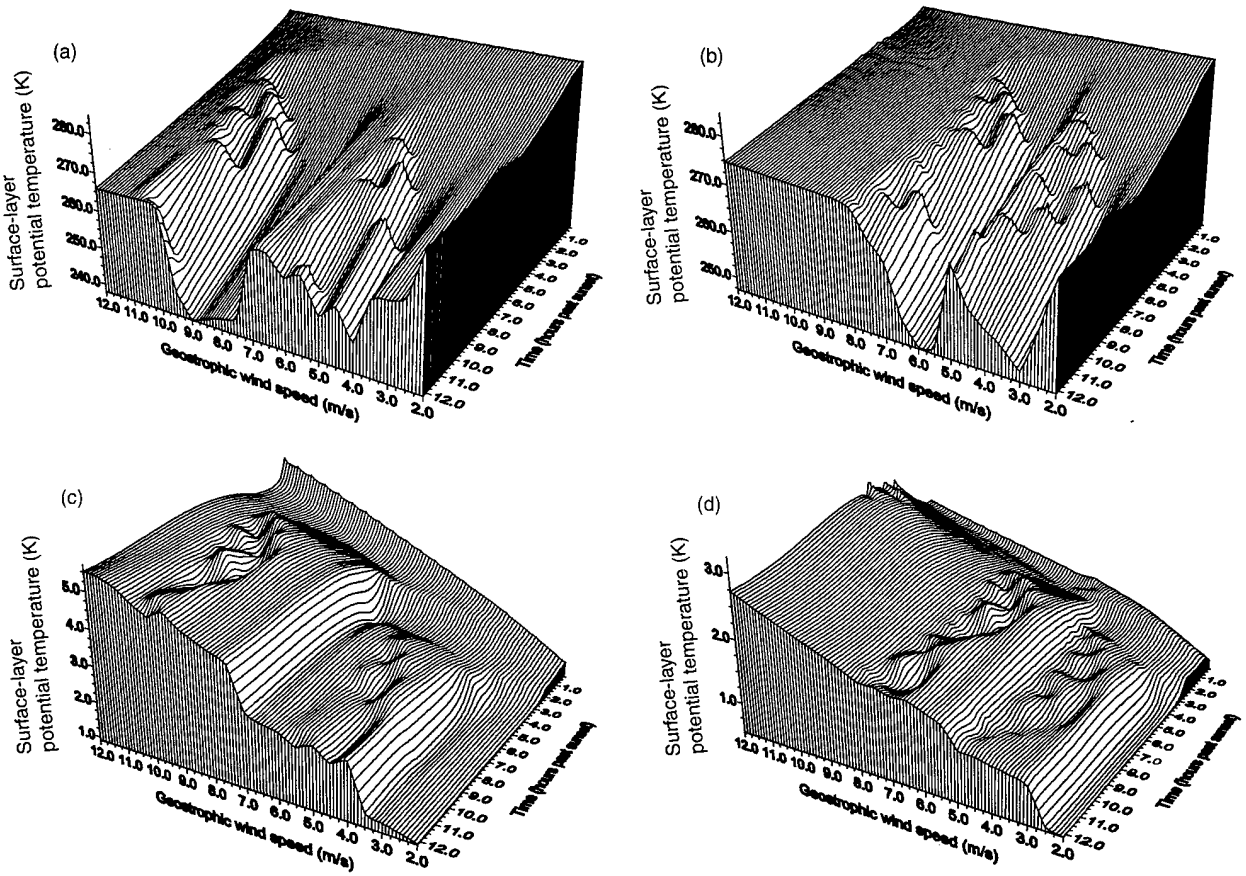

Figure 5. Surface plot of potential temperature (K) at 5 m agl in surface layer and wind speed (m/s) at 5 m agl in the surface layer as they are affected by changes in surface roughness (i.e., $z_0 = 0.01$ m (a) and (c) and $z_0 = 1.0$ m (b) and (d).

that turbulence is generated about 1.0 to 2.0 hours earlier and at 1.0 to 2.0 m/s lower geostrophic wind speeds as surface roughness increases. In other words, oscillations are more likely to occur over more rough (aerodynamically turbulent) surfaces with lower geostrophic wind speeds. The distribution and frequency of the oscillations also varies with changes in the roughness parameter. The numbers presented in parentheses in table 2 reflect these additional results.

Figure 6 is also similar to figure 2 except that it shows the model results as they are affected by changes in initial soil moisture, that is, $m_s = 0.05$ m^3/m^3 (fig. 6(a) and (c)) and $m_s = 0.20$ m^3/m^3 (fig. 6(b) and (d)). (In calculating the data in figure 2, $m_s = 0.10$ m^3/m^3.) These model results show that the surface layer tends toward warmer temperatures (approximately 2 to 3 K) as soil moisture increases. This is likely due to decreasing radiative losses and other surface-energy budget considerations (Munn, 1966). The results also show that the intensity of the oscillations increases for higher initial values of soil moisture, which is also an effect related to the heat capacity of the soil and surface cooling (see Lin, 1990).

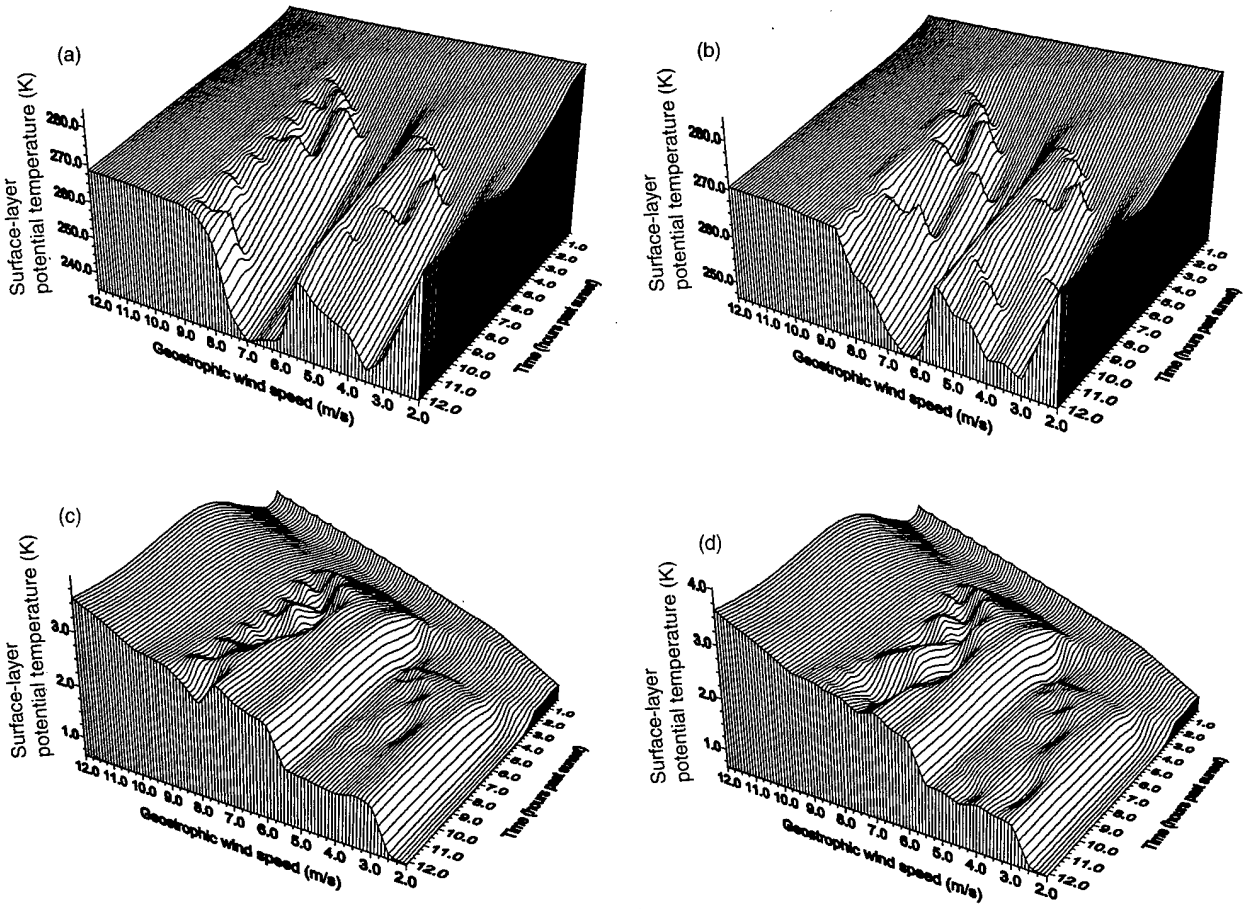

Figure 6. Surface plot of potential temperature (K) at 5 m agl in the surface layer (a) and (b) and wind speed (m/s) at 5 m agl in surface layer (c) and (d) as they are affected by changes in initial soil moisture (i.e., $m_S = 0.05$ m^3/m^3 (a) and (c) and $m_S = 0.20$ m^3/m^3 (b) and (d).

Figure 7(a), (b), and (c) shows the calculated momentum flux, $-\overline{u'w'} = K_m\sqrt{(\partial u/\partial z)^2 + (\partial v/\partial z)^2}$ in units of m^2/s^2, and heat flux, $-\overline{w'\theta'} = K_h(\partial\theta/\partial z)$ in figure 7(d), (e), and (f) in units of ms^{-1} K, in the lower boundary layer for levels of stability corresponding to three different initial values of geostrophic wind speed, that is, 6.5, 8.0, and 9.5 m/s. In the very stable layer case (fig. 7(a) and 7(d)), momentum increases through the lower boundary layer as the nocturnal low-level jet forms aloft. The model results show that the momentum flux continues downward through the lower boundary layer, even as the surface layer becomes increasingly more stable (and eventually laminar). This may explain why, in figure 1, the surface-layer wind speeds are around 2.5 m/s, rather than calm, through the nighttime period. In contrast, the heat flux through the laminar layer decreases as surface-layer temperatures (not shown) approach a kind of radiative equilibrium with the ground (Mahrt, 1998). Above the laminar layer ($z \geq 30$ m), the heat flux is nearly absent.

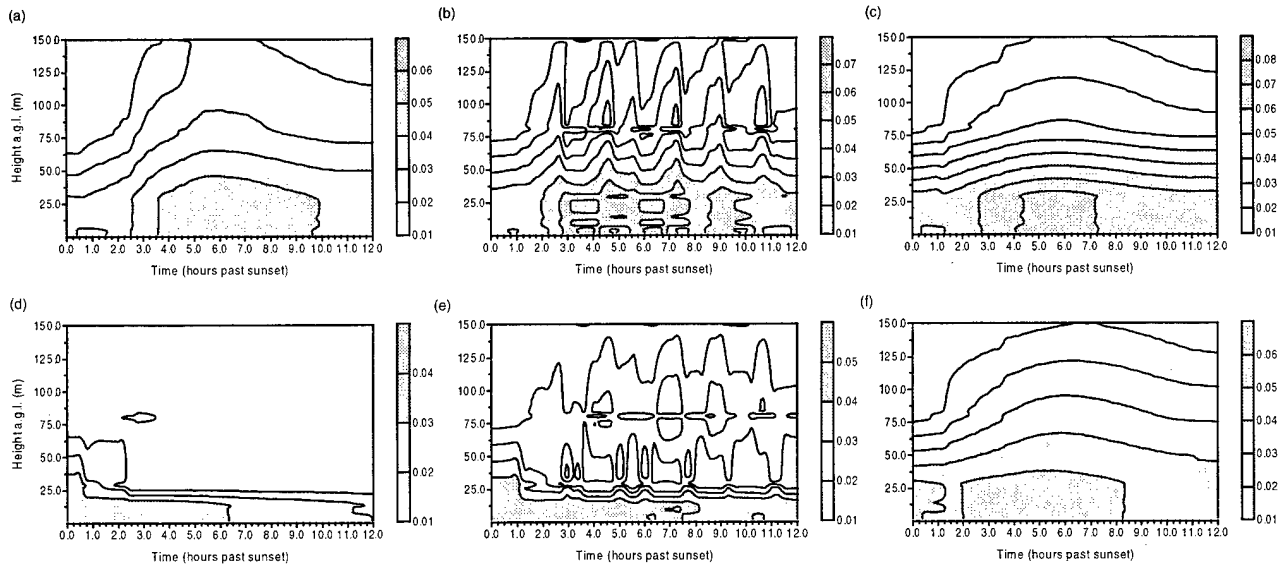

Figure 7. Contour plot of calculated momentum flux (a), (b), and (c) and heat flux (d), (e), and (f) through nighttime period for values of geostrophic wind speed of 6.5 (a) and (d), 8.0 (b) and (e), and 9.5 m/s (c) and (f).

In the intermittently stable case (fig. 7(b) and 7(e)), a series of sporadic breakdowns are shown as fluctuations of momentum and heat flux in the layer, $2 \leq z \leq 150$ m. There appear to be about 5 or 6 such events through the nighttime period. For this example, the surface roughness and initial geostrophic wind speed were 0.28 m and 8.0 m/s, respectively (same as fig. 1). Further analysis of these results would be desirable to provide additional information regarding the onset wind shear and thermal instabilities aloft.

In the weakly stable case (fig. (c) and (f)), both the heat and momentum flux remain strong through the nighttime period. The increased wind speeds (and wind shears) in this example do not permit the formation of a separate, highly stratified layer at the surface. Instead, the model derives a steady and much less severe decrease in temperatures (not shown) through the entire layer, that is, $2 \leq z \leq 150$ m. This is the coupled nighttime boundary-layer result.

4. Conclusion

In this study a computer atmospheric model is developed to simulate the lower nighttime stable-boundary layer. An overview is given for the development of wind shear and thermal stability in the lower boundary layer under weakly stable, highly stable, and intermittently stable conditions. Several graphs show incremental time series of the model data. They provide an improved and expanded view of the nighttime wind and temperature oscillations and of the parameter space within which such time-dependent oscillations occur. The model used in this study is shown to be a useful representation of the nighttime case that includes intermittent turbulence.

Acknowledgment

I would like to thank Ronald Meyers and Keith Deacon of the U.S. Army Research Laboratory for their comments on this study. I would also like to thank David Rosen of the U.S. Army Research Laboratory for reading through my report and for offering many helpful comments.

References

Ahlberg, J. H., E. N. Nilson, and J. L. Walsh (1967), *The Theory of Splines and Their Applications*. Academic Press, New York, 284 pp.

Avissar, R., and Y. Mahrer (1988), "Mapping frost-sensitive areas with a three dimensional local-scale numerical model. Part I: Physical and numerical aspects," *J. Appl. Meteorol.* **27**, pp. 400–413.

Blackadar, A. K. (1979), "High resolution models of the planetary boundary layer," in *Advances in Environmental Science and Engineering* **1**, J. Pfafflin and E. Ziegler, eds., Gordon and Breach, pp. 50-85.

Blumen, W., D. Fritts, and G. Poulos, eds. (1999), CASES-99 Overview and Experimental Design Plan, on internet at http://www.colorado-research.com/cases/C99Overview.html.

Businger, J. A. (1973), "Turbulent transfer in the atmospheric surface layer," in *Workshop on Micrometeorology*, D.A. Haugen, ed., American Meteorological Society, Boston, pp. 67–98.

Businger, J. A., J. C. Wyngaard, Y. Izumi, and E. F. Bradley (1971), "Flux-profile relationships in the atmospheric surface layer," *J. Atmos. Sci.* **28**, pp. 181–189.

Coulter, R. L. (1990), "A case study of turbulence in the stable nocturnal boundary layer," *Boundary-Layer Meteorol.* **52**, pp. 75–91.

Lin, J. T. (1990), *The effect of inertial and turbulence oscillations in the stable boundary layer and their role in horizontal dispersion*, M.S. thesis, Dept. of Mathematics, University of Alabama, Huntsville, 82 pp.

Lu, Nai-Ping, W.D. Neff, and J.C. Kaimal (1983), "Wave and turbulence structure in a disturbed nocturnal inversion," *Boundary-Layer Meteorol.* **26**, pp. 141–155.

Mahrt, L. (1998), "Stratified atmospheric boundary layers and breakdown of models," *Theoretical and Computational Fluid Dynamics* **11**, pp. 263–279.

McNider, R. T., and R. A. Pielke (1981), "Diurnal boundary-layer development over sloping terrain," *J. Atmos. Sci.* **38**, pp. 2198–2212.

McNider, R. T., D. E. England, M. J. Friedman, and X. Shi (1995), "Predictability of the stable atmospheric boundary layer," *J. Atmos. Sci.* **52**, pp. 1602–1614.

Monin, A. S., and A. M. Obukhov (1954), "Basic regularity in turbulent mixing in the surface layer of the atmosphere," *Akad. Nauk. S.S.S.R. Trud. Geofiz. Inst.* **24**, pp. 1963–1987.

Munn, R. E. (1966), *Descriptive Micrometeorology*, Academic Press, New York, 245 p.

Nappo, C. J. (1991), "Sporadic breakdown of stability in the PBL over simple and complex terrain," *Boundary-Layer Meteorol.* **54**, pp. 69–87.

Nappo, C. J., and W. D. Bach (1997), "Summary report on the ARO/ARL workshop on turbulence and diffusion in the stable boundary layer," *Bull. Am. Meteorol. Soc.* **78**, pp. 493–498.

Nappo, C. J., and P. Johansson (1998), "Summary report on the Lovanger international workshop on turbulence and diffusion in the stable boundary layer," *Bull. Am. Meteorol. Soc.* **79**, pp. 1401–1405.

Neff, W. D. (1980), *An observational and numerical study of the atmospheric boundary layer overlying the east arctic ice sheet*, Ph.D. thesis, Univ. of Colorado, Boulder, CO, 272 pp.

Paegle, J., W. G. Zdunkowski, and R. M. Welch (1976), "Implicit differencing of predictive equations of the boundary layer," *Mon. Weather Rev.* **104**, pp. 1321–1324.

Paltridge, G. W., and C.M.R. Platt (1976), *Radiative Processes in Meteorology and Climatology*, Elsevier, 318 pp.

Pielke, R. A. (1984), *Mesoscale Meteorological Modeling*, Academic Press, 612 pp.

Pielke, R. A., and Y. Mahrer (1975), "Representation of the heated planetary boundary layer in mesoscale models with coarse vertical resolution," *J. Atmos. Sci.* **32**, pp. 2288–2308.

Rachele, H., and A. Tunick (1994), "Energy balance model for imagery and electromagnetic propagation," *J. Appl. Meteorol.* **33**, pp. 964–976.

ReVelle, D. O. (1993), "Chaos and 'bursting' in the planetary boundary layer," *J. Appl. Meteorol.* **32**, pp. 1169–1180.

Schubert, J. F. (1977), "Acoustic detection of momentum transfer during the abrupt transition from laminar to a turbulent atmospheric boundary layer," *J. Appl. Meteorol.* **16**, pp. 1292–1297.

Smeda, M. S. (1979), "Incorporation of planetary boundary layer process into numerical forecast models," *Boundary-Layer Meteorol.* **16**, pp. 115–129.

Thorpe, A. J., and T. H. Guymer (1977), "The nocturnal jet," *Q. J. R. Meteorol. Soc.* **103**, pp. 633–653.

Tunick, A. (2000), *A One-Dimensional Atmospheric Boundary Layer Model: Comparison With Observations*, U.S. Army Research Laboratory, ARL-MR-484.

Tunick, A., H. Rachele, F. V. Hansen, J. A. Howell, J. L. Steiner, A. D. Schneider, and S. R. Evett (1994), "REBAL '92-A cooperative radiation and energy balance field study for imagery and E. M. propagation," *Bull. Am. Meteorol. Soc.* **75**, pp. 421–430.

Weber, A. H., and R. J. Kurzeja (1991), "Nocturnal planetary boundary-layer structure and turbulence episodes during the Project STABLE field program," *J. Appl. Meteorol.* **30**, pp. 1117–1133.

Zilitinkevich, S. (1970), *Dynamics of the Atmospheric Boundary Layer*, Leningrad, 291 pp.

Zhou, Ming-yu, Lu Nai-Ping, and Qu Shaohou (1980), "Applications of sodar data in weather analysis and local weather forecasting," *Kexue Tongbao* **25**, pp. 328– 331.

Appendix. Symbols

A	surface reflectivity (albedo)
cld	cloud amount (in tenths)
c_p	specific heat of air at constant pressure
f	Coriolis parameter
F	function applied in solving for the surface temperature through the surface-energy budget
g	acceleration due to gravity
k	Kármán's constant (~0.4)
K_h	eddy transfer coefficient for heat
K_m	eddy transfer coefficient for momentum
K_q	eddy transfer coefficient for moisture
l	mixing length
L_v	heat of transformation for water vapor
m_s	soil moisture or soil water content
q	specific humidity
q_*	surface-layer turbulence scaling parameter for moisture
Q_s	soil heat flux
Ri	ratio of thermal to mechanical (wind shear) production turbulent energy called the Richardson number
Ri_{crit}	limiting value of the Richardson number
$R_{s\downarrow}$	incoming solar radiative flux
$R_{L\downarrow}$	incoming long-wave radiative flux
$R_{L\uparrow}$	outgoing long-wave radiative flux
s	local wind shear,
t	time in hours past sunset
T_c	temperature of the cloud base (in kelvins)
T_r	reference level (~2 m) temperature (in kelvins)
u	east-west component of horizontal wind speed
u_g	east-west component of geostrophic wind speed
u_*	surface friction velocity
u'	eddy fluctuating component of the horizontal wind speed
v	north-south component of horizontal wind speed
v_g	north-south component of geostrophic wind speed
w'	eddy fluctuating component of the vertical wind speed
ε_c	emissivity of the cloud base
ϕ_h	nondimensional temperature lapse rate
ϕ_m	nondimensional wind shear
θ	potential temperature
θ	potential temperature scaling constant
ρ	air density
σ	Stefan-Boltzmann constant
$\overline{any}$	overbar denotes the mean

Distribution

Admnstr
Defns Techl Info Ctr
ATTN DTIC-OCP
8725 John J Kingman Rd Ste 0944
FT Belvoir VA 22060-6218

DARPA
ATTN S Welby
3701 N Fairfax Dr
Arlington VA 22203-1714

Mil Asst for Env Sci Ofc of the Undersec
of Defns for Rsrch & Engrg R&AT E LS
Pentagon Rm 3D129
Washington DC 20301-3080

Ofc of the Secy of Defns
ATTN ODDRE (R&AT)
The Pentagon
Washington DC 20301-3080

Ofc of the Secy of Defns
ATTN OUSD(A&T)/ODDR&E(R) R J Trew
3080 Defense Pentagon
Washington DC 20301-7100

ARL Chemical Biology Nuc Effects Div
ATTN AMSRL-SL-CO
Aberdeen Proving Ground MD 21005-5423

Natl Ground Intllgnc Ctr
Army Foreign Sci Tech Ctr
ATTN CM
220 7th Stret NE
Charlottesville VA 22901-5396

US Army Corps of Engrs
Engr Topographics Lab
ATTN CETEC-TR-G P F Krause
7701 Telegraph Rd
Alexandria VA 22315-3864

US Military Acdmy
Mathematical Sci Ctr of Excellence
ATTN MADN-MATH MAJ M Huber
Thayer Hall
West Point NY 10996-1786

Pac Mis Test Ctr Geophysics Div
ATTN Code 3250 Battalino
Point Mugu CA 93042-5000

Sci & Technlgy
101 Research Dr
Hampton VA 23666-1340

SMC/CZA
2435 Vela Way Ste 1613
El Segundo CA 90245-5500

US Army Avn & Mis Cmnd
ATTN AMSMI-RD-WS-PL G Lill Jr
Bldg 7804
Redstone Arsenal AL 35898-5000

US Army Combined Arms Combat
ATTN ATZL-CAW
FT Leavenworth KS 66027-5300

US Army CRREL
ATTN CRREL-GP R Detsch
72 Lyme Rd
Hanover NH 03755-1290

US Army Dugway Proving Ground
ATTN STEDP 3
ATTN STEDP-MT-DA-L-3
ATTN STEDP-MT-M Bowers
Dugway UT 84022-5000

US Army Field Artillery Schl
ATTN ATSF-TSM-TA
FT Sill OK 73503-5000

US Army Infantry
ATTN ATSH-CD-CS-OR E Dutoit
FT Benning GA 30905-5090

US Army Materiel Sys Anal Actvty
ATTN AMXSY-CS Bradley
Aberdeen Proving Ground MD 21005-5071

US Army OEC
ATTN CSTE-AEC-FSE
4501 Ford Ave Park Center IV
Alexandria VA 22302-1458

Distribution

US Army Spc Technlgy Rsrch Ofc
ATTN Brathwaite
5321 Riggs Rd
Gaithersburg MD 20882

US Army TACOM-ARDEC
ATTN AMSTA-AR-WEL-TL
Bldg 59 Phillips Rd
Picatinny Arsenal NJ 07806-5000

US Army Topo Engrg Ctr
ATTN CETEC-ZC
FT Belvoir VA 22060-5546

US Army TRADOC
ATTN ATCD-FA
FT Monroe VA 23651-5170

US Army TRADOC Anal Cmnd—WSMR
ATTN ATRC-WSS-R
White Sands Missile Range NM 88002

US Army White Sands Missile Range
ATTN STEWS-IM-ITZ Techl Lib Br
White Sands Missile Range NM 88002-5501

Nav Air War Ctr Wpn Div
ATTN CMD 420000D C0245 A Shlanta
1 Admin Cir
China Lake CA 93555-6001

Nav Rsrch Lab
ATTN Code 4110 Ruhnke
Washington DC 20375-5000

Nav Surfc Warfare Ctr
ATTN Code B07 J Pennella
17320 Dahlgren Rd Bldg 1470 Rm 1101
Dahlgren VA 22448-5100

Nav Surfc Weapons Ctr
ATTN Code G63
Dahlgren VA 22448-5000

AFCCC/DOC
ATTN Glauber
151 Patton Ave Rm 120
Asheville NC 28801-5002

Air Force
ATTN Weather Techl Lib
151 Patton Ave Rm 120
Asheville NC 28801-5002

Directed Energy Dirctrt
ATTN AFRL/DEBA
3550 Aberdeen Ave SE
Kirtland AFB NM 87117-5776

Hdqtrs AFWA/DNX
106 Peacekeeper Dr Ste 2N3
Offutt AFB NE 68113-4039

PL/WE
Kirtland AFB NM 87118-6008

TAC/DOWP
Langley AFB VA 23665-5524

USAF Rome Lab Tech
ATTN Corridor W Ste 262 RL SUL
26 Electr Pkwy Bldg 106
Griffiss AFB NY 13441-4514

NASA Marshal Spc Flt Ctr Atmos Sci Div
ATTN Code ED 41 1
Huntsville AL 35812

Colorado State Univ Dept of Atmos Sci
ATTN R A Pielke
FT Collins CO 80523

Iowa State Univ
ATTN R Arritt
312 Curtiss Hall
Ames IA 50011

Iowa State Univ
ATTN M Segal
2104 Agronomy Hall
Ames IA 50011-1010

Rutgers Univ-Cook Campus Envir & Natl
Resources Bldg
ATTN R Avissar
New Brunswick NJ 08903

Distribution

The City College of New York Dept of Earth & Atmos Sci
ATTN S D Gedzelman
J106 Marshak Bldg 137th and Covent Ave
New York City NY 10031

Univ of Alabama at Huntsville Rsrch Inst
ATTN R T Mcnider
Huntsville AL 35899

Agrclt Rsrch Svc Conserve & Prodn Rsrch Lab
ATTN T A Howell
PO Drawer 10
Bushland TX 79012

Dean RMD
ATTN Gomez
Washington DC 20314

Dept of Commerce
Ctr Mountain Administration
ATTN Spprt Ctr Library R51
325 S Broadway
Boulder CO 80303

Natl Ctr for Atmos Rsrch
ATTN NCAR Library Serials
PO Box 3000
Boulder CO 80307-3000

USDA Forest Svc Rocky Mtn Frst & Range Exprmnt Sta
ATTN K F Zeller
240 W Prospect Stret
FT Collins CO 80526

US Army Rsrch Lab
ATTN AMSRL-CI J D Gantt
ATTN AMSRL-CI-CB R Meyers
ATTN AMSRL-CI-EP A D Tunick
(13 copies)
ATTN AMSRL-CI-IS-R Mail & Records Mgmt
ATTN AMSRL-CI-IS-T Techl Pub (2 copies)
ATTN AMSRL-IS-EP Clark
ATTN AMSRL-SE-EE Z G Sztankay

REPORT DOCUMENTATION PAGE

Form Approved
OMB No. 0704-0188

1. AGENCY USE ONLY *(Leave blank)*	2. REPORT DATE	3. REPORT TYPE AND DATES COVERED
	June 2001	1/1/00–9/1/00

4. TITLE AND SUBTITLE A One-Dimensional Atmospheric Boundary Layer Model: Intermittent Wind Shears and Thermal Stability at Night

5. FUNDING NUMBERS
DA PR: B53A
PE: 61102A

6. AUTHOR(S) Arnold Tunick

7. PERFORMING ORGANIZATION NAME(S) AND ADDRESS(ES)
U.S. Army Research Laboratory
Attn: AMSRL-CI-EP email: atunick@arl.army.mil
2800 Powder Mill Road
Adelphi, MD 20783-1197

8. PERFORMING ORGANIZATION REPORT NUMBER
ARL-MR-494

9. SPONSORING/MONITORING AGENCY NAME(S) AND ADDRESS(ES)
U.S. Army Research Laboratory
2800 Powder Mill Road
Adelphi, MD 20783-1197

10. SPONSORING/MONITORING AGENCY REPORT NUMBER

11. SUPPLEMENTARY NOTES
ARL PR: 9FEJ70
AMS code: 611102.53A

12a. DISTRIBUTION/AVAILABILITY STATEMENT Approved for public release; distribution unlimited.

12b. DISTRIBUTION CODE

13. ABSTRACT *(Maximum 200 words)*

A one-dimensional, time-dependent computer model of the atmospheric boundary layer was developed to simulate intermittent turbulence and the near-ground microclimate under nighttime stable conditions. In this study, the model produced several turbulent events (oscillations) through the nighttime period that varied in number, frequency, and strength along the axes of initial geostrophic wind speed. These results were found to be in close agreement with results from several previous observational and theoretical studies of this type. It is suggested, therefore, that the one-dimensional computer model is a useful mathematical representation of the nighttime case that includes intermittency.

14. SUBJECT TERMS Descriptive meteorology, computer atmospheric model

15. NUMBER OF PAGES 32

16. PRICE CODE

17. SECURITY CLASSIFICATION OF REPORT	18. SECURITY CLASSIFICATION OF THIS PAGE	19. SECURITY CLASSIFICATION OF ABSTRACT	20. LIMITATION OF ABSTRACT
Unclassified	Unclassified	Unclassified	UL

NSN 7540-01-280-5500

Standard Form 298 (Rev. 2-89)
Prescribed by ANSI Std. Z39-18
298-102